IEEE Access
Multidisciplinary | Rapid Review | Open Access Journal

Received June 3, 2019, accepted July 1, 2019, date of publication July 8, 2019, date of current version July 25, 2019.

Digital Object Identifier 10.1109/ACCESS.2019.2927364

A Behavioral Model for Solar Cells With Transient Irradiation and Temperature Assessment

VICTOR RODOLFO GONZALEZ-DIAZ[1], (Member, IEEE), SERGIO ROMERO-CAMACHO[1], ROBERTO C. AMBROSIO-LAZARO[1], (Member, IEEE), GERARDO MINO-AGUILAR[1], (Member, IEEE), EDOARDO BONIZZONI[2], (Senior Member, IEEE), AND FRANCO MALOBERTI[2], (Fellow, IEEE)

[1]Faculty of Electronics, Benemérita Universidad Autónoma de Puebla (BUAP), Puebla 72000, Mexico
[2]Department of Electrical, Computer, and Biomedical Engineering, The University of Pavia, 27100 Pavia, Italy

Corresponding author: Victor Rodolfo Gonzalez-Diaz (vicrodolfo.gonzalez@correo.buap.mx)

This work was supported in part by the Vicerrectoria de Investigacion y Estudios de Posgrado (VIEP) BUAP and International Relationships Department through the DGDI/3232/2017 Student's Internship (2017-2018), and in part by the CONACyT, Mexico, under Project INFRA-2013-1-205873.

ABSTRACT The time to market of maximum power point tracking circuits for solar cells depends on the time of transient simulations. But, the traditional tools use a nonlinear resistor model for the solar cells. The question is if it is possible to use another nonlinear relationship to improve the convergence features. This paper presents a new method for modeling a solar cell, considering temperature and irradiation changes and an improved convergence performance. In this model, the solar cell's current-voltage (I-V) characteristics for three irradiation and two temperature conditions are required, showing a feasible procedure. The proposed model is fitted to three commercial solar cells exhibiting a maximum average error of 2.51 percent. It is tested in a transient analysis converging to the expected values in a maximum power point tracking circuit.

INDEX TERMS Solar cell, solar power generation, analytical models.

I. INTRODUCTION

Solar cells are important elements for the electronic circuit design flow. There are industrial software tools to design Photo-Voltaic (PV) systems [1]. However, some of the most important Computer Aided Design (CAD), for electronic circuit design, tools [2] do not include solar cells with the basic elements in the library setup. In these design platforms, it is not easy to construct a compatible solar cell model for low average error considering irradiation and temperature changes. For this limitation arises the need to explore the construction of solar cell models. Of the most recent and relevant solar cell models, it is possible to highlight three features: F1) the model considers irradiation (L) and temperature (T) changes, F2) uses linear functions to describe physics and F3) an extensive characterization to calculate implicit parameters.

The popular P-V design tools use the single and double diode description with up to five parameters [3]. The actual research focuses on new methods to obtain the 1-diode model parameters to fit the irradiation and temperature dependence [4]. There are several solar cell model parameter extraction methods, detailed in [5], [6]. The parameter extraction enables the construction of the most used models for solar cells [7]–[11].

The aforementioned are recent works solving the problem of modeling solar cells. The number of model parameters in the exponential functions increases to reduce the average error [7]. However, the size of the equation is a constraint when the solar cells are simulated together with other electrical elements. The 1-diode model is a nonlinear resistor with an exponential branch relationship. The question is if it is possible to use another nonlinear relationship to improve the convergence features. Particularly, the design of Maximum Power Point Tracking (MPPT) circuits gives rise to a critical situation [12]–[14]. It is necessary to test the tracking circuit with a solar cell model describing the physical parameters with the compatibility of an electronic circuit CAD. In this scenario, the behavioral description with VerilogA is a good option. This hardware description language is a reliable solution for the mixed signal electronic circuit design and reduces the time to market in many products.

The associate editor coordinating the review of this manuscript and approving it for publication was Lei Jiao.

This work extends the model in [15], which is a combination of physical analysis and a mathematical approach that considers temperature and irradiation effects. The proposed model needs the short circuit current, the open circuit voltage, and saturation conductance, for a few temperature and irradiation levels, which are feasible parameter measurements. It is important to notice that these parameters can also be obtained from the solar cell's datasheet, although in many cases they are not available. This is as standards have split content with mandatory and best practice information [16]. For instance: solar cells performance to different irradiance levels. Therefore, geographical locations and the split standard content makes some manufacturers give minimal information. The objective of this work is to give another option to model a solar cell achieving a good average error with the possibility to extract the parameters with a simple procedure. The manuscript is organized as follows: Section II details the necessary parameters and equations for the extended model. Section III compares the proposed model with the most recent solutions, including commercial solar cell curves in transient analyses in an MPPT circuit. Finally, Section IV draws conclusions.

II. THE PROPOSED SOLAR CELL MODEL

A. MODEL DESCRIPTION

The proposed model is a set of linearized equations considering the irradiation and temperature variations. The model requires the voltages and currents associated with three irradiation and two temperature levels, which are feasible measurements from the I-V characteristics. Additionally, it is possible to obtain the set of values from the solar cell's datasheet [11]. This Section details the process to construct the model.

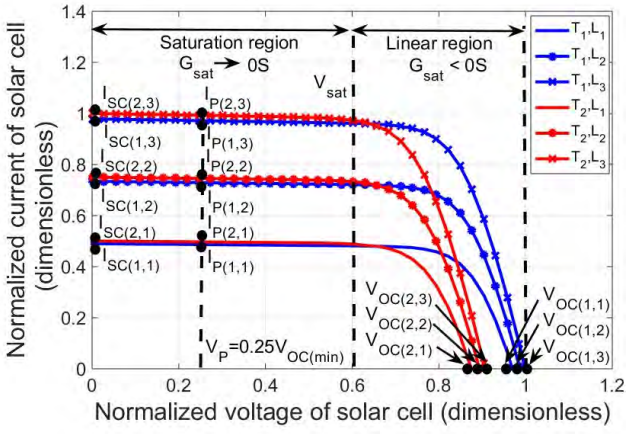

FIGURE 1. I-V characteristic curves corresponding to three irradiation and two temperature levels, where blue and red curves belong to T_1 and T_2, respectively.

Fig. 1 shows the solar cell's current-voltage (I-V) characteristic curves, corresponding to three irradiation and two temperature levels. Taking I_{PV}, V_{PV} as the solar cell current and voltage, the curves have a nonlinear relationship. However, it is possible to distinguish two regions of operation. For $V_{PV} > V_{sat}$, I_{PV} has an approximately linear dependence on V_{PV}. This region of operation is well described by a constant and negative G_{lin}. In fact, the following analysis shows that the saturation conductance depends mostly on irradiance in a nonlinear relationship. The saturation region corresponds to $V_{PV} \leq V_{sat}$, where I_{PV} is approximately constant and independent of V_{PV}. Therefore, the conductance G_{sat} in this region will be considered zero.

The family curves have three important parameters: the short circuit current I_{sc} with $V_{PV} = 0$, open circuit voltage V_{oc} with $I_{PV} = 0$ and the saturation voltage V_{sat} limiting the two regions of operation. The proposed model in this work requires the I-V characteristic for three irradiation and two temperature levels.

Let three irradiation levels in Fig. 1 to be $L_1 < L_2 < L_3$, two temperature levels $T_1 < T_2$ and I_p as a current probe associated to a quarter of the minimum open circuit voltage, i.e., $V_p = V_{oc(min)}/4$. Fig. 1 highlights with black dots the short circuit current I_{sc}, open circuit voltage V_{oc} and current probe I_p. The measurements associated with any irradiation and temperature compose the three matrices:

$$I_{sc(j,k)} = \begin{bmatrix} I_{sc(1,1)} & I_{sc(1,2)} & I_{sc(1,3)} \\ I_{sc(2,1)} & I_{sc(2,2)} & I_{sc(2,3)} \end{bmatrix} \quad (1)$$

$$V_{oc(j,k)} = \begin{bmatrix} V_{oc(1,1)} & V_{oc(1,2)} & V_{oc(1,3)} \\ V_{oc(2,1)} & V_{oc(2,2)} & V_{oc(2,3)} \end{bmatrix} \quad (2)$$

$$I_{p(j,k)} = \begin{bmatrix} I_{p(1,1)} & I_{p(1,2)} & I_{p(1,3)} \\ I_{p(2,1)} & I_{p(2,2)} & I_{p(2,3)} \end{bmatrix}. \quad (3)$$

In eqns. (1)-(3), the (j, k) index is for $T_1 < T_2 < \cdots < T_j$ temperature and $L_1 < L_2 < \cdots < L_k$ irradiation levels.

It is possible to approximate the solar cell current by a hyperbolic tangent function, used on a Current Limiter Matlab-Simulink module. An important property, compared to the 1-diode model is that this function has a limited codomain and is monotonous along with the I-V values. This feature improves convergence in transient simulations. For the model, the variables depending on irradiation and temperature are the short circuit current, the open circuit voltage and the conductance in the saturation region. The general expression for I_{PV} is:

$$I_{PV} = I_{sc} \tanh(X_1) + |G_{sat}|(V_{oc} - V_{PV}) \quad (4)$$

$$X_1 = K_t(V_{oc} - V_{PV})/V_{sat}, \quad (5)$$

where K_t is a coefficient of proportionality defining the linear region curvature. The model uses the strategies in [17] for the I_{sc}, V_{oc}, and G_{sat} equations.

Note that the proposed model is a hyperbolic relationship between the solar cell's I-V curve and takes the saturation conductance from the average slope in the short circuit current point. However, the I_{sc}, G_{sat}, V_{oc} nonlinear behavior is simplified with a linear curve fitting for a small set of irradiation and temperature cases. The following subsections describe the procedure to obtain these parameters, to construct the model equation.

B. SHORT CIRCUIT CURRENT I_{SC}

The short circuit current is a feasible measurement in most solar cell configurations. Figures 2 and 3 show a typical I_{sc} characterization as a function of irradiation and temperature levels. It is possible to describe it with a simple linear relationship.

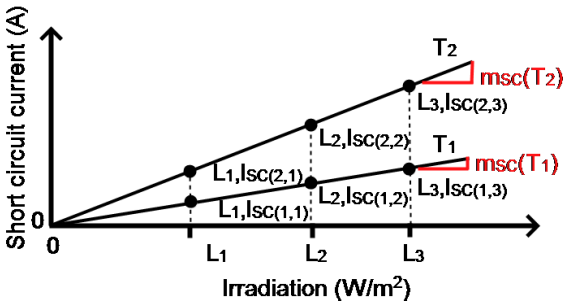

FIGURE 2. Short circuit current as a function of the irradiation, for two temperature levels.

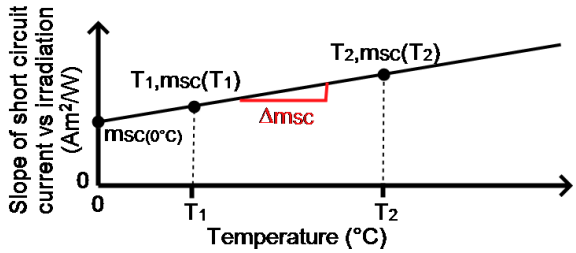

FIGURE 3. Short circuit linearization as a function of temperature. The slope of short-circuit current, as a function of T.

$$I_{sc} = m_{sc}(T)L, \tag{6}$$

where L is the irradiation level, T the temperature and $m_{sc}(T)$ the slope of $I_{sc}(L)$, a function of T. The term $m_{sc}(T)$ has a physical feature which is possible to describe with:

$$m_{sc}(T) = m_{sc(0°\mathrm{C})} + \Delta m_{sc} T. \tag{7}$$

The term $m_{sc(0°\mathrm{C})}$ is the slope at 0°C and Δm_{sc} is the slope of m_{sc} as a function of T. With the present data in matrix $I_{sc(j,k)}$, $m_{sc(0°\mathrm{C})}$ and Δm_{sc} are:

$$m_{sc}(T_1) = (I_{sc(1,3)} - I_{sc(1,1)})/(L_3 - L_1) \tag{8}$$
$$m_{sc}(T_2) = (I_{sc(2,3)} - I_{sc(2,1)})/(L_3 - L_1) \tag{9}$$
$$\Delta m_{sc} = (m_{sc}(T_1) - m_{sc}(T_2))/(T_1 - T_2) \tag{10}$$
$$m_{sc(0°\mathrm{C})} = m_{sc}(T_1) - \Delta m_{sc} T_1. \tag{11}$$

C. OPEN CIRCUIT VOLTAGE V_{OC}

The Figures 4 and 5 show V_{oc} as function of irradiation and temperature levels. The curves are plotted with information from the solar cell's datasheet. Approximately, the open circuit voltage has a linear dependence on temperature and

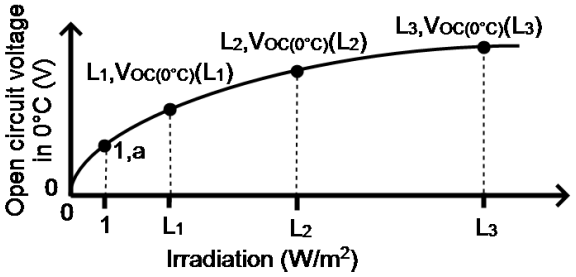

FIGURE 4. Open circuit voltage at 0°C as a function of the irradiation, where potential fitting is used.

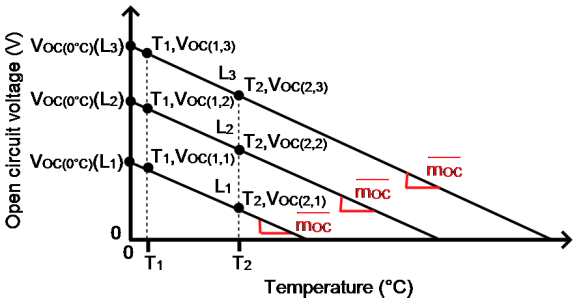

FIGURE 5. Open circuit voltage as a function of temperature, for three irradiation levels.

a nonlinear relationship with irradiation. A curve fitting approximation is possible in the following form:

$$V_{oc} = V_{oc(0°\mathrm{C})}(L) + \overline{m_{oc}} T \tag{12}$$

where $\overline{m_{oc}}$ is the average slope of $V_{oc}(T)$, $V_{oc(0°\mathrm{C})}(L)$ is a power function that defines the open circuit voltage at 0°C. The term $V_{oc(0°\mathrm{C})}(L)$ is approximated by potential fitting, whose general equation is:

$$V_{oc(0°\mathrm{C})}(L) = aL^b. \tag{13}$$

With data of matrix, $V_{oc(j,k)}$, $\overline{m_{oc}}$ is calculated as:

$$\overline{m_{oc}} = \frac{1}{3}\sum_{k=1}^{3} \frac{V_{oc(1,k)} - V_{oc(2,k)}}{T_1 - T_2}. \tag{14}$$

For $V_{oc(0°\mathrm{C})}(L)$, the potential fitting is the following:

$$V_{oc(0°\mathrm{C})}(L_1) = V_{oc(1,1)} - \overline{m_{oc}} T_1 \tag{15}$$
$$V_{oc(0°\mathrm{C})}(L_2) = V_{oc(1,2)} - \overline{m_{oc}} T_1 \tag{16}$$
$$V_{oc(0°\mathrm{C})}(L_3) = V_{oc(1,3)} - \overline{m_{oc}} T_1 \tag{17}$$
$$S_1 = \sum_{n=1}^{3} (\log L_n)[\log V_{oc(0°\mathrm{C})}(L_n)] \tag{18}$$
$$S_2 = \sum_{n=1}^{3} \log L_n \tag{19}$$
$$S_3 = \sum_{n=1}^{3} \log V_{oc(0°\mathrm{C})}(L_n) \tag{20}$$

$$S_4 = \sum_{n=1}^{3} [\log(L_n)]^2 \tag{21}$$

$$\overline{L'} = S_2/3 \tag{22}$$

$$\overline{V_{oc(0°C)}(L)'} = S_3/3 \tag{23}$$

$$b = (3S_1 - S_2S_3)/(3S_4 - S_2^2) \tag{24}$$

$$a' = \overline{V_{oc(0°C)}(L)'} - b\overline{L'} \tag{25}$$

$$a = 10^{a'}. \tag{26}$$

D. SATURATION CONDUCTANCE

The proposed model expresses the saturation conductance for two temperature and three irradiation levels. Similarly to (1)–(3), the saturation conductance matrix is:

$$G_{sat(j,k)} = \begin{bmatrix} G_{sat(1,1)} & G_{sat(1,2)} & G_{sat(1,3)} \\ G_{sat(2,1)} & G_{sat(2,2)} & G_{sat(2,3)} \end{bmatrix}. \tag{27}$$

The matrix $G_{sat(j,k)}$ is therefore defined as:

$$G_{sat(j,k)} = -4(I_{sc(j,k)} - I_{p(j,k)})/V_{oc(min)}. \tag{28}$$

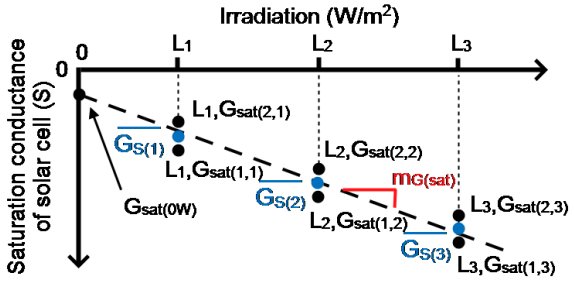

FIGURE 6. Solar cell's saturation conductance as a function of irradiation.

Fig. 6 shows the G_{sat} linearization as a function of irradiation. For any irradiation level, there is a pair of conductance values (black dots) corresponding to temperatures T_1 and T_2. The saturation conductance is a strong function of irradiation, rather than temperature. Therefore, it is possible to ignore the G_{sat} temperature dependence. For any irradiation level, the proposed model calculates the average conductance in saturation (blue dots) at temperatures T_1 and T_2. The average conductance for k-th irradiation is:

$$\overline{G_{s(k)}} = (G_{sat(1,k)} + G_{sat(2,k)})/2, \tag{29}$$

with $k = 1, 2, 3$. The general equation of the saturation conductance is the following:

$$G_{sat} = G_{sat(0\mathrm{W})} + m_{G(sat)}L, \tag{30}$$

where $m_{G(sat)}$ is the slope of $G_{sat}(L)$, and $G_{sat(0\mathrm{W})}$ is the saturation conductance when the irradiation is 0W/m^2. Such terms are calculated by linear fitting, resulting in the following equations:

$$m_{G(sat)} = \frac{3\sum_{n=1}^{3} L_n\overline{G_{s(n)}} - \sum_{n=1}^{3} L_n \sum_{n=1}^{3} \overline{G_{s(n)}}}{3\sum_{n=1}^{3} L_n^2 - (\sum_{n=1}^{3} L_n)^2} \tag{31}$$

$$G_{sat(0W)} = \frac{\sum_{n=1}^{3} \overline{G_{s(n)}} - m_{G(sat)} \sum_{n=1}^{3} L_n}{3}. \tag{32}$$

The model is constructed using eqn. (30), (12), (6) in eqn. (4). It is possible to describe the proposed model in many hardware description languages. This work uses the VerilogA behavioral description in Cadence Virtuoso [2]. The data required by this algorithm are the aforementioned irradiation and temperature measurements, resulting in the description of $I_{sc(j,k)}$, $V_{oc(j,k)}$ and $I_{p(j,k)}$. These matrices are uncorrelated and easily obtained in a single step.

The prospected model is another option when it is not possible to find the necessary information to consider temperature dependence. It considers the $I_{sc}(L, T)$, $V_{oc}(L, T)$, $G_{sat}(L, T)$ parameters correcting not only temperature, but also irradiation dependence on the same equations. This correlation improves the average error as the results in the next section show.

III. RESULTS AND ANALYSIS

A. EXPERIMENT AND RESULTS

The prospected model is validated describing three solar cells: the MX Solar USA MX60-220, Sanyo Electric of Panasonic Group HIP 186DA3 and Sharp ND-62RU1. The solar cells are simulated with Spectre in Cadence Virtuoso to compare with physical data extracted from PV array blocks in Matlab-Simulink. Figures 7–12 show the comparison of the proposed model with experimental data as a function of irradiation and temperature levels.

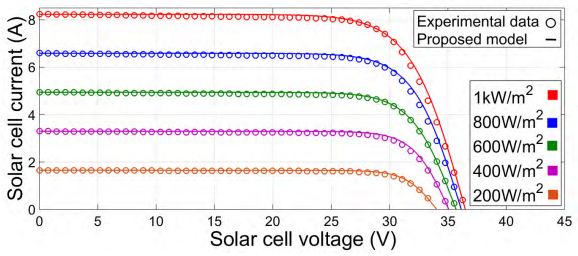

FIGURE 7. MX Solar USA MX60-220 characteristic curves: Current-voltage curves, for five irradiation levels, at 25° C.

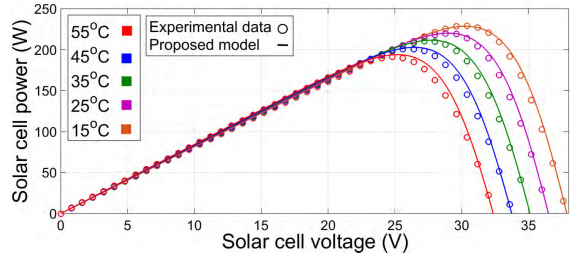

FIGURE 8. MX Solar USA MX60-220 characteristic curves: Power-voltage curves, for five temperature levels, for 1 kW/m^2.

Based on the procedure described in Section II, the saturation conductance requires the voltage V_p. The set of values for this experiment are $V_p = \{7.53\mathrm{V}, 14.5\mathrm{V}, 2.29\mathrm{V}\}$,

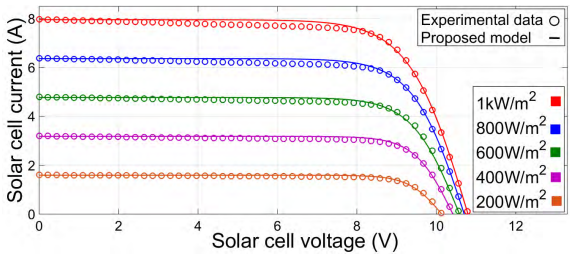

FIGURE 9. Sharp ND-62RU1 characteristic curves: Current-voltage curves, for five irradiation levels, at 25° C.

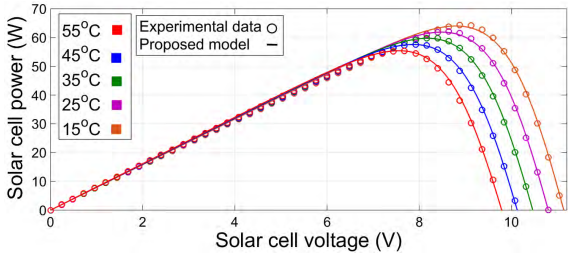

FIGURE 10. Sharp ND-62RU1 characteristic curves: Power-voltage curves, for five temperature levels, for 1 kW/m^2.

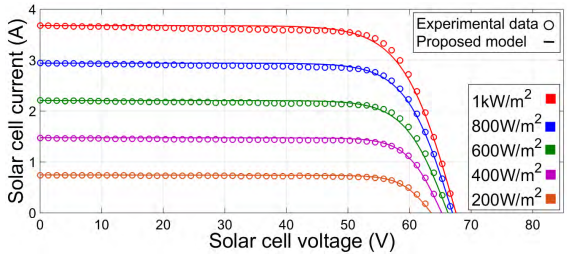

FIGURE 11. Sanyo Electric of Panasonic Group HIP-186DA3 characteristic curves. Current-voltage curves, for five irradiation levels, at 25° C.

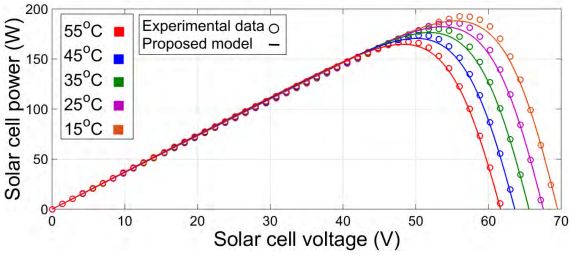

FIGURE 12. Sanyo Electric of Panasonic Group HIP-186DA3 characteristic curves Power-voltage curves, for five temperature levels, for 1 kW/m^2.

corresponding to the model for MX Solar, Sanyo and Sharp respectively. The set of values change according to the solar cell voltages of operation. The saturation voltage V_{sat} and K_t coefficient are key elements to fit curves around the saturation voltage in I-V curves and maximum power point PV curves in Fig. 7–12. The saturation voltage was defined as $V_{sat} = 0.7V_{oc(max)}$ and takes values of $V_{sat} = \{26.6\text{V}, 49\text{V}, 8.4\text{V}\}$, for models MX Solar, Sanyo and Sharp respectively. The coefficient of proportionality is $K_t = \{10, 8.7, 7, 6.5, 5.7\}$, for irradiation levels from 200W/m^2 to 1kW/m^2, with step size of 200W/m^2.

The numerical results of the model and experimental data are compared for validation. This is for three different temperature and three different irradiation levels. The average error is estimated with the expression [4]:

$$\xi(X) = \frac{1}{N}\sum_{i=1}^{N}\left|\frac{X_m(i) - X_c(i)}{X_m(i)}\right| \times 100 \qquad (33)$$

where $X_m(i)$ are the proposed model I-V curve points and $X_c(i)$ the experimental results. Table 1 shows the average errors between the simulated and the experimental data for IV curves with each irradiation level. For the MX Solar model, the maximum average error occurs at 400W/m^2 and for Sanyo, is at 200W/m^2. For Sharp models, the minimum errors occur from 800W/m^2 to 1kW/m^2. For the Sanyo and Sharp models, the absolute error reduces with the increase of irradiation levels.

TABLE 1. The average errors of I-V characteristic curves corresponding to five irradiation levels @ 25°C.

	Irradiation (W/m^2)				
Model	**200**	**400**	**600**	**800**	**1k**
MX Solar	1.48	1.63	1.13	1.58	1.50
Sanyo	2.37	2.11	2.17	1.40	1.48
Sharp	2.47	2.23	2.51	1.57	1.67

TABLE 2. The average errors of power-voltage characteristic curves corresponding to five temperature levels @ 1 kW/m^2.

	Temperature (°C)				
Model	**15**	**25**	**35**	**45**	**55**
MX Solar	1.43	1.40	1.48	1.67	1.84
Sanyo	1.49	1.48	1.38	1.27	1.14
Sharp	1.75	1.57	1.46	1.38	1.36

Table 2 shows the average errors between the proposed model and the experimental data, for P-V curves at different temperature levels. For the MX Solar model, the maximum average error occurs at 55°C, and for Sanyo, this occurs at 15°C. For Sharp solar cells, the average errors decrease as temperature increases.

These results validate the proposed model with typical operating conditions. The errors are less than 2.51%, and the maximum errors locate between the saturation and open circuit conditions. This is the result of a dependence on the K_t parameter for the saturation voltage curvature. Therefore, if K_t increases, the transition from saturation to the linear region is more abrupt. K_t increases when the irradiation level decreases in an asymptotic manner. The second cause of average errors is the saturation voltage approximation since it exhibits a slight dependence on irradiation and temperature.

The accuracy of the proposed model results from the equations (6) and (12), for short circuit current and open circuit voltage respectively. Tables 3 and 4 show the relative

percentage errors of such approaches. The relative percentage error is defined as:

$$\%\text{err} = \left| \frac{X_{\text{meas}} - X_{\text{model}}}{X_{\text{meas}}} \right| \times 100 \qquad (34)$$

TABLE 3. The relative error of the proposed short circuit current equation as a function of irradiation.

	Irradiation (W/m^2)				
Model	**200**	**400**	**600**	**800**	**1k**
MX Solar	0.37	0.03	0.06	0.04	0.01
Sanyo	1.04	0.16	0.12	0.13	0.05
Sharp	0.69	0.50	0.38	0.26	0.14

TABLE 4. The relative error of the proposed open circuit voltage equation as a function of temperature.

	Temperature (°C)				
Model	**15**	**25**	**35**	**45**	**55**
MX Solar	0.01	0.01	0.11	0.23	0.25
Sanyo	0.10	0.01	0.10	0.21	0.33
Sharp	0.01	0.11	0.11	0.23	0.24

For the short circuit current equation, with the sole exception of Sanyo solar cell in 200W/m^2, all relative errors are less than 1.04%. In all cases, the tendency is the reduction of relative error if irradiation increases. Thus, the data in Table 3 confirms (6), i.e., the short circuit current is directly proportional to the irradiation level, for any constant temperature level. For the open circuit voltage equation, all relative errors are less than 0.24%, with the tendency of an increment of the relative error if temperature increases. Therefore, the data in Table 4 confirms eqn. (14). There are only a few publications considering the irradiation and temperature effects with simple procedures [4] and the presented results are compared with the most recent solutions. Note that considering the irradiation changes is not the same procedure of shading effects. For shading, it is necessary to consider a Photo Voltaic array configuration with the solar cell model in this work.

B. APPLICATION IN TRANSIENT SIMULATIONS OF PV HARVESTING SYSTEM

The proposed model is used to perform transient simulations of a Photo Voltaic energy harvesting system. Fig. 13 shows the schematic representation having three principal elements:

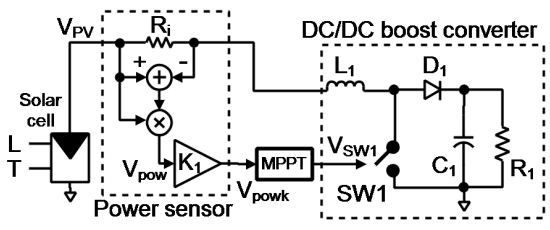

FIGURE 13. The configuration of the solar cell model, power sensor, DC/DC boost converter and MPPT circuit used for transient analysis.

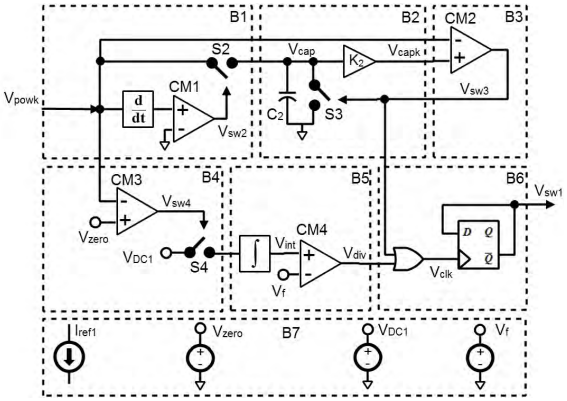

FIGURE 14. The MPPT circuit architecture.

a power sensor circuit, a DC-DC boost converter and the Maximum Power Point Tracking system (MPPT). The values for the DC/DC boost converter and power sensor are: $R_1 = 220\Omega$, $L_1 = 1.5$mH, $C_1 = 220\mu$F and $K_1 = 13.5$. The testbench uses the proposed solar cell model in VerilogA with the Sanyo Electric of Panasonic Group HIP-186DA3 parameters. The MPPT circuit follows the solar cell operation at its maximum point [21]. It is a hierarchical system consisting of the entities in Fig. 14. The systems' discontinuous nature sets critical conditions for transient simulations. The MPPT instances are transistor level circuits with a CMOS 65nm technology. Table 5 summarizes the name, the function and the number of transistors of each block.

TABLE 5. Description of the used MPPT entities.

Block	Function	Devices
Positive slope detector (B1)	Sends V_{powk} to B2, switching S2 when V_{powk} is rising and interrupts it in opposite case.	30
Hold-attenuation circuit (B2)	Holds and attenuates V_{cap} by a factor K_2 if S3 is open.	2
Limit falling detector (B3)	$V_{SW3} = 1$ if $V_{capk} > V_{powk}$ to close switch S3.	30
Zero power detector (B4)	S4 is closed if $V_{powk} < V_{zero}$.	30
Integrator (B5)	$V_{div} = 1$ if $V_{int} > V_f$ after a $20\mu s$ integration time.	21
State memory (B6)	$V_{SW1} = 1$ if V_{clk} is rising, where $V_{clk} = 1$ if $(V_{div}\ OR\ V_{SW3}) = 1$.	42
Bias circuit (B7)	Generates current and voltage references for blocks B1 to B6.	9

Fig. 15 shows the transient result for a step irradiation change from 600 − 300 W/m^2 in a 400 μs time lapse. The proposed model reaches the maximum power point P_{MPP}, which is 112.11 W for 600W/m^2 and 54.35W for 300W/m^2. The maximum power corresponding to 600W/m^2 is twice the maximum power corresponding to 300W/m^2. The aforementioned is because, if the saturation conductance effect is ignored, the solar cell power is directly proportional to the irradiation level. Note that even with this discontinuous irradiation, the model and circuits always converge to

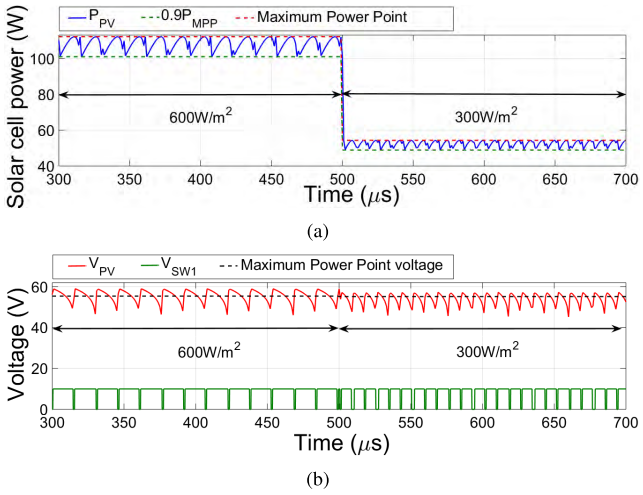

FIGURE 15. Transient response with a Sanyo Electric of Panasonic Group HIP-186DA3, with variable irradiation at a constant temperature of 25°C. a) Solar cell power. b) Solar cell voltage.

the P_{MPP}. The MPPT circuit fulfills its function and keeps the power ripple oscillation between P_{MPP} and $0.9P_{MPP}$ for all conditions with no convergence problems. The maximum power point voltage is the value corresponding to P_{MPP}, resulting in 55.17V for 300W/m^2 and 55.39V for 600W/m^2, a difference of 220mV. This means that the maximum power point voltage does not change significantly if the irradiation level changes with constant temperature, as PV curves show. This physical behavior is expected and is included in the model with eqn. (12).

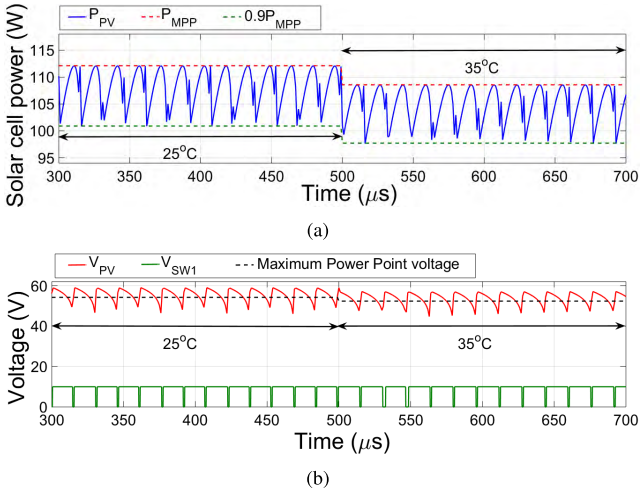

FIGURE 16. Transient response with a Sanyo Electric of Panasonic Group HIP-186DA3, with variable temperature and constant irradiation of 600W/m^2. a) Solar cell power. b) Solar cell voltage.

Another test with temperature dependence helps to validate the convergence model. Figure 16 shows the transient simulation with a temperature sweep from $25-35$°C in a 400 μs time lapse. The P_{MPP} is 112.11W for 25°C and 108.57W for 35°C. The power difference between the two previous temperature levels is 3.54W. As it was for the transient response with step irradiation, the step temperature variation does not generate convergence problems. These results verify the functionality of the model for robust applications. The maximum power point voltage is 54.21V for 25°C and 52.36V for 35°C; this is an expected result with a 3.53% of change. In a range of 10°C, the maximum power and maximum power point voltage do not change significantly if the temperature level changes and irradiation is constant.

C. COMPARISON WITH RECENT MODELS

Table 6 summarizes the recent solar cell models with the highlighted features in Section I. The previous models show a trade-off with linearity and characterization of intrinsic parameters to adjust to the experimental data. It is possible to evaluate the performance of several 1-diode based models compared with the proposed. Not all 1-diode models include irradiance dependence. The proposed model presents a good average error and is competitive even if most of the reported models only present relative and absolute errors. There is a trade-off between computational budget and quantity of average error.

TABLE 6. Comparison of the recent solar cell models.

Model	Method	Features			Error
		F1 T and L	F2 Linear	F3 Charac.	
[12]	MOSFET-based (1-diode model)	Partially	Yes	Yes	not indicated
[7]	PWL (PIN diode based)	Partially	Partially	Yes	relative error $< 0.25\%$
[8]	Nonlinear system (1-diode model)	Yes	No	Yes	absolute error $< 1\%$
[9]	Curve fitting (two diodes)	No	No	Yes	absolute error $< 0.9\%$
[10]	Numerical approximation (1-diode model)	No	Yes	Partially	not indicated
[18]	Continuity equation (multiple devices)	Partially	No	No	1% relative error
[19]	Fuzzy system (exponential junction current)	Yes	No	No	1% MSE
[20]	Device level (1-diode model)	Partially	No	No	not indicated
[4]	Single diode model	Yes	Yes	No	average error $< 10\%$
This work	**Irradiation and Temperature linearization**	**Yes**	**Yes**	**Yes**	**average error** $< 2.51\%$

The proposed model considers irradiation and temperature changes with a simple linearized set of equations. It is possible to obtain the I_{sc}, V_{oc}, G_{sat} parameters from the manufacturer's datasheets or this can be obtained with a small number of measurements. The model presents a balance in the

desired features with a maximum average error of 2.51%. It is important to mention that the previous models in VerilogA do not report transient simulations [20].

The model fits the experimental data with a low average error, compared with the most recent solutions. The big difference is the possibility of describing the model in VerilogA to launch simulations in a full custom circuit design environment.

IV. CONCLUSION

The results of this work show that it is possible to construct a behavioral model for solar cells with three important features: using linear functions, considering irradiation/temperature effects, and employing explicit model parameters. The I-V and P-V characteristic curve compared with the model and the experimental data exhibit an absolute error of less than 2.51%. The short circuit current is directly proportional to the irradiation, whose coefficient of proportionality is determined by temperature. The open circuit voltage has a linear dependency on temperature, whose rate of change is always negative and constant. The results validate the linearized equations, requiring minimal measurements for the proposed model.

The proposed model is appropriate for transient tests in stringent conditions of irradiation and temperature. The model fits a variety of circuits, such as power converters and control stages, in behavioral, schematic or layout level. The proposed model easily translates into other languages. In platforms for integrated circuit design, the model offers the capability of making transition tests, where irradiation and temperature change.

REFERENCES

[1] S. A. PVsyst. *PVsyst: Software for Study Simulation Photovoltaic Systems*. Accessed: Nov. 8, 2018. [Online]. Available: www.pvsyst.com

[2] Cadence Design Systems. *Virtuoso Analog Design Environment XL*. Accessed: Sep. 27, 2018. [Online]. Available: https://www.cadence.com/

[3] N. Femia, G. Petrone, and M. Vitelli, *Power Electronics and Control Techniques for Maximum Energy Harvesting in Photovoltaic Systems*. Boca Raton, FL, USA: CRC Press, 2013.

[4] Y. Chaibi, M. Salhi, A. El-Jouni, and A. Essadki, "A new method to extract the equivalent circuit parameters of a photovoltaic panel," *Solar Energy*, vol. 163, no. 1, pp. 376–386, Mar. 2018.

[5] S. Yadir, S. Assal, A. E. Rhassouli, M. Sidki, and M. Benhmida, "A new technique for extracting physical parameters of a solar cell model from the double exponential model (DECM)," *Opt. Mater.*, vol. 36, no. 1, pp. 18–21, Nov. 2013.

[6] X. Chen, K. Yu, W. Du, W. Zhao, and G. Liu, "Parameters identification of solar cell models using generalized oppositional teaching learning based optimization," *Energy*, vol. 99, pp. 170–180, Mar. 2016. [Online]. Available: http://www.sciencedirect.com/science/article/pii/S0360544216000827

[7] A. Ortiz-Conde, D. Lugo-Muñoz, and F. J. García-Sánchez, "An explicit multiexponential model as an alternative to traditional solar cell models with series and shunt resistances," *IEEE J. Photovolt.*, vol. 2, no. 3, pp. 261–268, Jul. 2012.

[8] D. Stefan, "Matlab/Simulink solar cell model based on electrical parameters at only one operating condition," in *Proc. 18th Int. Conf. Syst. Theory, Control Comput. (ICSTCC)*, Oct. 2014, pp. 709–714.

[9] S. Yadir, H. Amiry, R. Bendaoud, A. E. Hassnaoui, A. Obbadi, M. Benhmida, and M. E. Aydi, "Physical parameters extraction by a new method using solar cell models with various ideality factors," in *Proc. 27th Int. Conf. Microelectron. (ICM)*, Dec. 2015, pp. 323–326.

[10] R. Tai, B. Y. Chen, and F. X. Chen, "Parameter extraction for single-diode model of solar cell," in *Proc. Int. Conf. Ind. Inform.-Comput. Technol., Intell. Technol., Ind. Inf. Integr. (ICIICII)*, Dec. 2016, pp. 319–322.

[11] A. Laudani, F. R. Fulginei, and A. Salvini, "High performing extraction procedure for the one-diode model of a photovoltaic panel from experimental I–V curves by using reduced forms," *Solar Energy*, vol. 103, no. 1, pp. 316–326, May 2014.

[12] R. Mahto, P. Zarkesh-Ha, and O. Lavrova, "MOSFET-based modeling and simulation of photovoltaics module," in *Proc. IEEE 43rd Photovoltaic Spec. Conf. (PVSC)*, Jun. 2016, pp. 3078–3081.

[13] E. Scolari, F. Sossan, and M. Paolone, "Photovoltaic-model-based solar irradiance estimators: Performance comparison and application to maximum power forecasting," *IEEE Trans. Sustain. Energy*, vol. 9, no. 1, pp. 35–44, Jan. 2018.

[14] J. Ahmed and Z. Salam, "A modified P&O maximum power point tracking method with reduced steady-state oscillation and improved tracking efficiency," *IEEE Trans. Sustain. Energy*, vol. 7, no. 4, pp. 1506–1515, Oct. 2016. doi: 10.1109/TSTE.2016.2568043.

[15] S. Romero-Camacho, V. R. Gonzalez-Diaz, R. C. Ambrosio-Lazaro, G. Mino-Aguilar, E. Bonizzoni, and F. Maloberti, "A new linearized behavioral model for solar cells," in *Proc. IEEE Int. Conf. Environ. Elect. Eng. IEEE Ind. Commercial Power Syst. Eur. (EEEIC/I&CPS)*, Jun. 2017, pp. 1–6.

[16] *Marking and Documentation Requirements for Photovoltaic Modules*, Standard EN 50380:2017, BSI, Sep. 2017.

[17] D. D. Mooney and R. J. Swift, *A Course in Mathematical Modeling*. Washington, DC, USA: Mathematical Association of America, 1999.

[18] A. Lopes, A. Araújo, A. Mendes, and L. Andrade, "A dye-sensitized solar cell model implementable in electrical circuit simulators," *Solar Energy*, vol. 122, no. 1, pp. 169–180, Dec. 2015.

[19] A. Chikh and A. Chandra, "Adaptive neuro-fuzzy based solar cell model," *IET Renew. Power Gener.*, vol. 8, no. 6, pp. 679–686, Aug. 2014.

[20] S. Dongaonkar, X. Sun, M. Lundstrom, and M. A. Alam. (Oct. 2014). *TAG Solar Cell Model (p-i-n Thin Film)*. [Online]. Available: https://nanohub.org/publications/20/1

[21] S. Romero-Camacho, V. R. Gonzalez-Diaz, R. C. Ambrosio-Lazaro, G. Mino-Aguilar, E. Bonizzoni, and F. Maloberti, "An improved analog maximum power point tracking circuit for solar cells suitable for abrupt variations in irradiation levels," in *Proc. IEEE Int. Conf. Environ. Elect. Eng IEEE Ind. Commercial Power Syst. Eur. (EEEIC/I&CPS)*, Jun. 2017, pp. 1–6.

VICTOR RODOLFO GONZALEZ-DIAZ was born in Puebla, Mexico. He received the M.Sc. and Ph.D. degrees from the National Institute for Astrophysics, Optics and Electronics (INAOE), Puebla, Mexico, in 2005 and 2009, respectively. He collaborated as a Postdoctoral Fellow at the Microsystems Laboratory, The University of Pavia, Italy, from 2009 to 2010. Since 2011, he is Full Time Professor with the Faculty of Electronics, BUAP, Puebla. His main research interests include frequency synthesizers, data converters, and sigma–delta modulation for analog and digital applications.

SERGIO ROMERO-CAMACHO was born in Puebla, Mexico. He received the B.Sc. in electronics and the M.Sc. degree from the Faculty of Electronics, Benemérita Universidad Autónoma de Puebla, in 2014 and 2017, respectively. He has involved in the generation of pseudo-random sequences in integrated circuits and synthesis of digital circuits in CAD tools. Recently, he developed research in the design of power management circuits with analog and mixed-signal circuits design.

ROBERTO C. AMBROSIO-LAZARO was born in Oaxaca, Mexico, in 1973. He received the B.S. degree in electronic engineering from the Faculty of Electronics, Technological Institute of Oaxaca, Oaxaca, in 1997, and the M.S. and Ph.D. degrees in microelectronics from the National Institute of Astrophysics, Optics and Electronics, Puebla, Mexico, in 2000 and 2005, respectively. He is currently a Researcher with the Electronics School, Meritorious Autonomous University of Puebla. His research interests include energy harvesting devices and systems, and integration of semiconductors materials for the development of solar cells and sensors.

GERARDO MINO-AGUILAR was born in Puebla, Mexico, 1971. He received the bachelor's degree in electronics engineering at Benemérita Universidad Autónoma de Puebla, in 1995, the master's degree in power electronics from the Universidad de las Américas Puebla, in 1999, and the Ph.D. degree in control of electrical machines from the Universitat Politècnica de Catalunya, Spain, in 2006. Since 2009, he has been the Head of the Power Electronics Systems for Drives, Power Quality and Energy Generation Research Group. He is currently the Head of the Graduate Department of Electronics Faculty, BUAP. His research interests include digital systems, power electronics, power quality, power generation, electric drives, and drivetrain electric vehicles.

EDOARDO BONIZZONI (SM'18) was born in Pavia, Italy, in 1977. He received the Laurea degree *(summa cum laude)* in electronic engineering and the Ph.D. degree in electronic, computer, and electrical engineering, with a focus on development, design, and testing of non-volatile memories with particular regard to phase-change memories, from The University of Pavia, Italy, in 2002 and 2006, respectively, where he is currently an Associate Professor with the Department of Electrical, Computer, and Biomedical Engineering. He has authored or coauthored over 120 papers in international journals or conferences (with published proceedings) and two book chapters. His current research interests include design and testing of DC-DC and A/D converters. He has focused on single-inductor multiple-output dc–dc buck regulator solutions and on both the Nyquist-rate and oversampled A/D converters. His research focuses on the design of high-precision amplifiers and ultra-low-voltage voltage reference circuits as well. He was a co-recipient of the IEEE ISCAS 2014 Honorary Mention Paper Award of the Sensory Systems Track, the IEEE/IEEJ Analog VLSI Workshop 2010 Best Paper Award, the IEEE European Solid-State Circuits Conference 2007 Best Paper Award, and the IEEE/IEEJ Analog VLSI Workshop 2007 Best Paper Award. From 2011 to 2015, he has served as an Associate Editor for the IEEE TRANSACTIONS ON CIRCUITS AND SYSTEMS-PART II of the IEEE Circuits and Systems Society. He has been an Associate Editor of the IEEE TRANSACTIONS ON CIRCUITS AND SYSTEMS-PART I, since 2016.

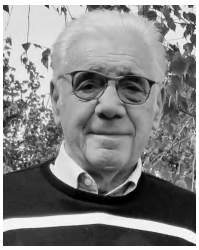

FRANCO MALOBERTI (M'84–SM'87–F'96–LF'16) received the Laurea degree *(summa cum Laude)* in physics from the University of Parma, Italy, and the Dr. Honoris Causa degree in electronics from Inaoe, Puebla, Mexico. He was a Visiting Professor with ETH-PEL, Zürich, and EPFL-LEG, Lausanne. He was the TI/J. Kilby Analog Engineering Chair Professor with the Texas A&M University and the Distinguished Microelectronic Chair Professor with The University of Texas at Dallas. He is currently an Emeritus Professor with The University of Pavia, Italy. He is an Honorary Professor with the University of Macau, China. He also is the Chairman of the Academic Committee of the AMSV State Key Laboratory, Macau, China. His professional expertise is in the design, analysis, and characterization of integrated circuits and analogue digital applications, mainly in the areas of switched capacitor circuits, data converters, interfaces for telecommunication and sensor systems, and CAD for analog and mixed A-D design. He has authored or coauthored more than 600 published papers and seven books. He holds 38 patents. He received the 1999 IEEE CAS Society Meritorious Service Award, the 2000 CAS Society Golden Jubilee Medal, and the IEEE Millenium Medal. He also received the 1996 IEE Fleming Premium, the ESSCIRC 2007 Best Paper Award, and the IEEJ Workshop 2007, and 2010 Best Paper Award. He also received the IEEE CAS Society 2013 Mac Van Valkenburg Award. He was the VP of the Region 8 of the IEEE CAS, from 1995 to 1997, an Associate Editor of the IEEE-TCAS-II, the President of the IEEE Sensor Council, from 2002 to 2003, an IEEE CAS BoG Member, from 2003 to 2005, and the VP of IEEE CAS, from 2007 to 2008. He was the Past President of the IEEE CAS Society, from 2017 to 2018, and the President, from 2015 to 2016. He was a DL of the IEEE SSC Society, from 2009 to 2010, and the IEEE CAS Society, from 2006 to 2007 and from 2012 to 2013.